Title

Application of Climate Projections and Monte Carlo Approach for Assessment of Future River Flow: Khorramabad River Basin, Iran

Journal

Journal of Hydrologic Engineering, 24(7)

ISSN

1084-0699

Authors

Moghadam, Seyedeh Hadis

Ashofteh, Parisa-Sadat

Loáiciga, Hugo A

Publication Date

2019-07-01

DOI

10.1061/(asce)he.1943-5584.0001801

Peer reviewed

Case Study

Application of Climate Projections and Monte Carlo Approach for Assessment of Future River Flow: Khorramabad River Basin, Iran

Seyedeh Hadis Moghadam[1]; Parisa-Sadat Ashofteh[2]; and Hugo A. Loáiciga[3]

Abstract: This paper assesses the impact of climate change uncertainties on the Khorramabad River basin's runoff in Lorestan Province, Iran. Five atmosphere-ocean general circulation models' (AOGCMs) [Hadley Centre Coupled Model, version 3 (HadCM3), Center for Climate System Research-National Institute for Environmental Studies (CCSR-NIES), Commonwealth Scientific and Industrial Research Organization Mark 2 (CSIRO-MK2), Coupled Global Climate Model (CGCM2), and Geophysical Fluid Dynamics Laboratory (GFDL-R30)] projections of rainfall and surface temperature were applied to simulate climate in the periods 2040–2069 and 2070–2099 under the A2 and B2 greenhouse gases (GHGs) emissions scenarios. The AOGCM projections showed an increase in temperature and a decrease in rainfall over the future periods. The ranges of climate change scenarios were determined, and the models' results were weighted for each month based on the *k*-nearest neighbors (KNN) method. Multiple time series of temperature and rainfall were generated with the Monte Carlo method based on their monthly probability distributions. The identification of unit hydrographs and component flows from the rainfall, evapotranspiration, and streamflow (IHACRES) hydrological model was calibrated and validated, and subsequently applied to simulate future river flow with downscaled climatic data from (1) five AOGCMs, and (2) a developed Monte Carlo model. The results showed that the average annual long-term runoff calculated with the developed Monte Carlo approach in the period 2040–2069 under the A2 and B2 scenarios decreased by 7.76% and 10.63%, respectively. The average annual runoff decreased by 13.06% and 29.49%, respectively, relative to the baseline period in the period 2070–2099 under the A2 and B2 scenarios. These results indicate a worsening availability of runoff through the remainder of the 21st century in the study region. **DOI: 10.1061/(ASCE)HE.1943-5584.0001801.**

Author keywords: Climate change; Uncertainty; Monte Carlo model; Simulation laboratory (SIMLAB) software; River flow.

Introduction

Human-induced emissions of greenhouse gases (GHGs) in the post–Industrial Revolution era are suspected of altering climatic patterns of hydrologic importance (IPCC 2007). These impacts may have adverse consequences on the economy, the environment, and other sectors. Multiple publications on modern-era climate change runoff impacts have appeared over the last 30 years.

Prudhomme et al. (2003) described a methodology for quantifying uncertainties of climate change impacts. Uncertainties were calculated with a set of 25,000 climate scenarios randomly generated by Monte Carlo simulation, and employing several general circulation models (GCMs). Flow series representative of current and future conditions were simulated using a conceptual hydrological model. Mimikou et al. (2001) determined climate change impacts on the quantity and quality of streamflow with the use of a physically based rainfall-runoff model and an in-stream model. Ekström et al. (2005) applied results from the HadRM3H model [following the IPCC (2000) (SRES) Scenario A2 for 2070–2100] to assess possible changes in extreme rainfall across the United Kingdom using regional frequency analysis and individual grid box analysis. Wilby and Harris (2006) presented a probabilistic framework for assessing uncertainties in climate change impacts for the River Thames, United Kingdom. They weighted the GCM results according to an index of reliability for downscaled effective rainfall. A Monte Carlo approach was then employed to explore the components of uncertainty affecting projections by 2080. The results indicated that cumulative distribution functions (CDFs) of low flows were most sensitive to uncertainty in the climate change scenarios and the downscaling of different GCMs. Sidhu et al. (2011) assessed climate change impacts and management strategies for sustainable water-energy-agriculture outcomes in Punjab, India. Shah Karami et al. (2011) evaluated the uncertainties of seven atmosphere-ocean GCM (AOGCM) models with the A2 emissions scenario for the Zayandeh Rud basin during two periods (2010–2039 and 2070–2099). They estimated the probability distributions of possible changes in rainfall and temperature. The impacts of these changes on water resources and agricultural indices were evaluated. Nazif et al. (2012) investigated the changes in snowmelt and consequent changes in runoff under two specific climate change scenarios in northwestern Tehran. The effect of climate change on daily temperature extreme values under the A2 and B2 emissions scenarios were simulated with the Hadley Centre Coupled Model, version 3 (HadCM3). Ahmadi et al. (2014) applied the HadCM3 climate model to project temperature and precipitation for early (2025–2039), middle (2055–2069), and late (2085–2099) periods under the A2 emission scenario. The estimated

[1]M.Sc. Student, Dept. of Civil Engineering, Univ. of Qom, 3716146611 Qom, Iran. Email: sh.moghadam@stu.qom.ac.ir

[2]Assistant Professor, Dept. of Civil Engineering, Univ. of Qom, 3716146611 Qom, Iran (corresponding author). Email: ps.ashofteh@qom.ac.ir

[3]Professor, Dept. of Geography, Univ. of California, Santa Barbara, CA 93016-4060. Email: hloaiciga@ucsb.edu

Note. This manuscript was submitted on April 6, 2018; approved on February 4, 2019; published online on April 26, 2019. Discussion period open until September 26, 2019; separate discussions must be submitted for individual papers. This paper is part of the ***Journal of Hydrologic Engineering***, © ASCE, ISSN 1084-0699.

climatic data were input to the identification of unit hydrographs and component flows from rainfall, evapotranspiration, and streamflow (IHACRES) model to simulate inflow to the Karoon-4 reservoir in Iran. A metaheuristic multiobjective optimization algorithm, the nondominated sorting genetic algorithm II (NSGA-II), was implemented to optimize dynamic operation rules in the Karoon-4 reservoir. Chithra and Thampi (2015) employed five general circulation models to calculate downscaled monthly precipitation data. Ashofteh et al. (2016b) evaluated the performance of AOGCM projections of temperature and rainfall in a base period (1971–2000) in the Aidoghmoush Basin, Iran, calculated with seven AOGCMs. The monthly time series of temperature and rainfall resulting from AOGCMs in the base period were input to a calibrated hydrological model. The mean observed runoff (MOR) weighting method was employed to assess the effectiveness of each climate model. Ashofteh et al. (2013) assessed the impacts of climate change on river flow and water demand in an eastern Azerbaijan river basin. Zamani et al. (2017) presented an approach to investigate the resiliency of the Jarreh Reservoir in southwestern Iran for the period 2025–2054 using a probabilistic technique under climate change. Sarzaeim et al. (2017) proposed data-mining algorithms for runoff projection under climate change conditions. The genetic programming (GP), artificial neural network (ANN), and support vector machine (SVM) data-mining tools were applied to project runoff in the Aidoghmoush Basin, Iran.

Several recent works dealing with the development and application of computational techniques in hydrologic engineering are cited next. Cheng et al. (2005) calibrated a multiple-criteria rainfall-runoff model using a parallel genetic algorithm in a cluster of computers. Chau (2007) developed a split-step particle swarm optimization (PSO) model and applied it to train multilayer perceptrons for forecasting real-time water levels in the Shing Mun River, Hong Kong. Wu and Chau (2011) implemented rainfall-runoff modeling using artificial neural networks coupled with singular spectrum analysis (SSA). Taormina et al. (2015) compared the performance of modular models (MMs) and global models (GMs) at nine gauging stations in the northern United States. Gholami et al. (2015) simulated groundwater level fluctuations in an alluvial aquifer of the Caspian southern coasts, Iran, by means of dendrochronology (tree rings) and an ANN for the period from 1912 through 2013. Fotovatikhah et al. (2018) reported a comprehensive survey of the application of computational intelligence-based methods in flood-management systems.

Iran features a dry and semiarid climate that may bear negative impacts of climate change. Various studies have been carried out on the likely effects of climate change in Iran. Most of them have ignored the role of climate change uncertainties. This paper assesses the effect of climate change uncertainties on the flow of the Khorramabad River, Iran. First, temperature and rainfall climate data for the baseline period (1971–2000) and future periods (2040–2069) and (2070–2099) are calculated with AOGCMs under the IPCC A2 and B2 emission scenarios. Our method evaluates the effect of uncertainties in the AOGCM projections with a model based on the Monte Carlo approach. The Khorramabad River flow is projected based on the IHACRES rainfall-runoff model (which has relative low input requirements, is driven by observed temperature and rainfall, and has been shown to rely on a relatively simple and efficient computational algorithm). The IHACRES model receives climatic inputs from several AOGCMs and the developed Monte Carlo model under the A2 and B2 emission scenarios. The projections are for the periods 2040–2069 and 2070–2099. In summary, this work develops a river-flow projection model based on the Monte Carlo approach considering the uncertainties in the AOGCMs' climatic predictions.

Methodology

This paper's methodology applies GHG emissions and climatic scenarios by downscaling AOGCM projections, weighting the model's outputs, and conducting uncertainty analysis and rainfall-runoff modeling. A flowchart of this paper's tasks is depicted in Fig. 1.

Creating Future Climate Scenarios

AOGCMs are the most advanced tools for making climate projections (Lane et al. 1999; Michell 2003; Wilby and Harris 2006). This paper implements five AOGCMs' projections for this purpose: the CSIRO Atmospheric Research Mark 2 climate model (CSIRO-MK2), the Coupled General Circulation Model 2 (CGCM2), the Centre for Climate System Research-National Institute for Environmental Studies (CCSR-NIES) model, HadCM3, and the Geophysical Fluid Dynamics Laboratory (GFDL) GFDL-R30 model (IPCC-TGCIA 1999). The IPCC Third Assessment Report (IPCC 2001) (TAR) climate change scenarios are adopted in this work. The Third Assessment Report considered seven AOGCMs: HadCM3, CCSR-NIES, CGCM2, CSIRO MK2, GFDL R30, ECHAM4, and National Center for Atmospheric Research/Department of Energy/Parallel Climate Model (NCAR DOE PCM). The ECHAM4 and NCAR DOE PCM models do not simulate temperature and rainfall in the study region (due to poor performance in simulating climatic variables compared with observed data), and therefore were not considered herein.

Emission Scenarios

Changes in the concentrations of GHGs in the Earth's atmosphere modify the atmosphere's radiative balance, which impacts multiple Earth processes. The future concentrations of GHGs produced

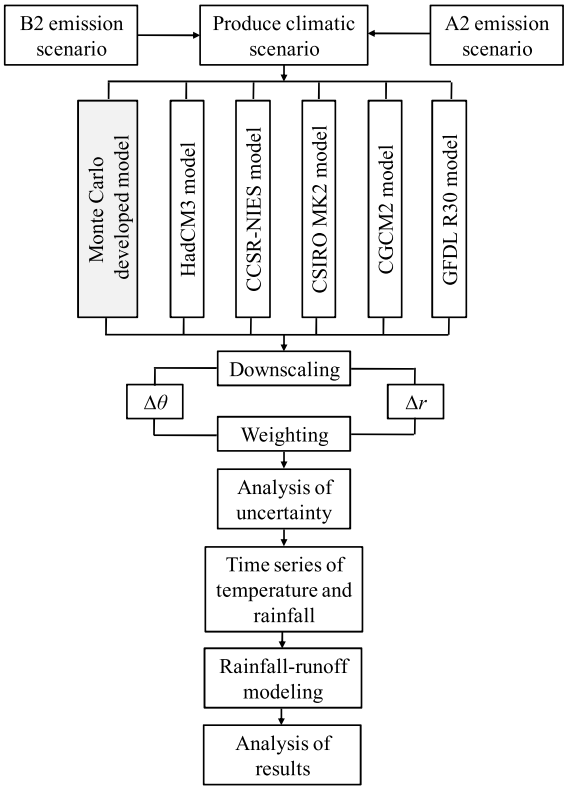

Fig. 1. Flowchart of methodology tasks.

J. Hydrol. Eng., 2019, 24(7): 05019014

by humans are uncertain, and those are projected under distinct scenarios. These scenarios include a wide range of future population and economic growth. Among the emission scenarios are B1, A2, A1, and B2 (Nakicenovic and Swart 2000).

The A2 emissions scenario envisions high regional population growth and relatively low dependence on rapid economic progress. The A1 scenario envisions a world with fast economic and population growth, with economic issues taking precedence over the environment. The B2 scenario emphasizes regional solutions to strengthen economic, social, and environmental issues. The B1 scenario is similar to A1 for population growth but places more emphasis on the use of clean energies, economic sustainability, and the environment. The A2 and B2 emission scenarios were chosen in this study because the former prescribes relatively high GHGs emissions and the later conforms well with possible future economic conditions in Iran.

Climate Change Scenarios

Comparison of AOGCM climate projections with observed data in regional basins shows that there are differences between observations and projections. A comparison of the long-term average of projected variables with observed values indicates a better accuracy of the AOGCM projections of long-term average climate variables. For these reasons, the average predictions of climate variables by AOGCMs are used in modeling future hydrologic conditions (Jones and Hulme 1996). Previous studies indicated that a statistically suitable period for projecting climate change signals is on the order of 30 years (Wilby and Harris 2006; Ashofteh et al. 2016a).

The average climate change scenario is written in terms of temperature difference in Eq. (1), whereas the average climate change scenario for precipitation is written in terms of a ratio in Eq. (2)

$$\Delta\theta_m = (\bar{\theta}_{\mathrm{AOGCM,fut},m} - \bar{\theta}_{\mathrm{AOGCM,bas},m}) \tag{1}$$

$$\Delta r_m = \left(\frac{\bar{r}_{\mathrm{AOGCM,fut},m}}{\bar{r}_{\mathrm{AOGCM,bas},m}}\right) \tag{2}$$

in which $\Delta\theta_m$ and Δr_m = the climate change scenarios corresponding to temperature and rainfall averaged over 30 years for each month ($1 \le m \le 12$), respectively; $\bar{\theta}_{\mathrm{AOGCM,fut},m}$ = 30-year average temperature projected by the AOGCMs in the future periods for each month (here, 2040–2069 and 2070–2099); $\bar{\theta}_{\mathrm{AOGCM,bas},m}$ = average 30-year temperature projected by the AOGCMs in the observed or baseline period (1971–2000) for each month; $\bar{r}_{\mathrm{AOGCM,fut},m}$ = 30-year average rainfall projected by the AOGCMs in the future periods for each month; and $\bar{r}_{\mathrm{AOGCM,bas},m}$ = average 30-year rainfall simulated by the AOGCMs in the observed or baseline period for each month.

Downscaling of Climate Projections

The construction of regional climate scenarios from AOGCMs larger-scale projections is called downscaling. Downscaling can be spatial and temporal. This study employs the method of interpolation of the adjacent cells to downscale spatially. This method eliminates inconsistency in the variations between projected climatic variables at nearby sites that are located in different computational cells (Barrow et al. 1996). Research shows that for interpolation calculations, at least four cells surrounding the interpolated cell are needed (von Storch et al. 1993). This work employs the change factor method for temporal downscaling. The latter method adds the climate change scenarios of $\Delta\theta_m$ and Δr_m to the observed values (1971–2000) as follows (Wilby and Harris 2006):

$$\theta_t = (\theta_{\mathrm{obs},t} + \Delta\theta_{m,t}) \tag{3}$$

$$r_t = (r_{\mathrm{obs},t} \times \Delta r_{m,t}) \tag{4}$$

in which θ_t and r_t = projected time series of temperature and rainfall, respectively; and $\theta_{\mathrm{obs},t}$ and $r_{\mathrm{obs},t}$ = time series of monthly temperature and rainfall observed in the baseline period, respectively ($1 \le t \le 360$ for 30 years of monthly analysis).

Monte Carlo Approach for Uncertainty Analysis

The uncertainties encountered in the prediction of climate change impacts render predictions uncertain themselves. One of these uncertainties arises from the greenhouse gaseous emissions scenarios. This is because of the complex nature of socioeconomic evolution. Another uncertainty arises from the AOGCMs simulations because these models are imperfect representations of the earth system. Different AOGCMs produce different climatic projections for the same region due to their process representation, parameterization, and downscaling algorithms.

Monte Carlo simulation methods analyze the effect of uncertainties on the output of a system's model. The uncertainties in $\Delta\theta$ and Δr resulting from AOGCMs and those of the emissions scenarios cast doubt on deterministic climatic projections. Instead, it is preferable to construct probabilistic distributions of climatic projections in an attempt to capture their uncertainties. To accomplish this, $\Delta\theta$ and Δr are treated as random variables subjected to Monte Carlo simulation with which to calculate probability distribution functions for basin runoff.

Weighting of AOGCM projections would best characterize climate-change impacts on runoff. This paper implements the k-nearest neighbors (KNN) weighting method, whereby AOGCMs projections are weighted based on the difference between the average of projected climatic variables over the baseline period and the average of observed data

$$W_{m,i} = \frac{\frac{1}{CV_{m,i}}}{\sum_{i=1}^{I} \frac{1}{CV_{m,i}}} \tag{5}$$

in which $CV_{m,i}$ = difference between the average of climate variables (temperature and rainfall) simulated in the baseline period with model i and the respective average for month m from the average observed data; $W_{m,i}$ = weight of each model i corresponding to the average long-term month m; and I = total number of AOGCMs (here, $I = 5$).

The effect of AOGCM uncertainties on river runoff was tackled with the Monte Carlo approach by generating 100 climate projections with Eqs. (1) and (2) and Simulation Laboratory (SIMLAB) software (Giglioli and Saltelli 2003). SIMLAB is designed for Monte Carlo–based uncertainty and sensitivity analysis. The computational steps of the SIMLAB are as follows (Giglioli and Saltelli 2003):

1. A range and probability distribution function are selected for each input factor. These selections are used in the next step in the generation of a sample from the input factors. If the analysis is primarily of an exploratory nature then approximate distribution assumptions may be adequate.
2. A sample of points is generated from the distribution of the inputs specified in the first step. The result of this step is a sequence of sample elements.
3. The sample elements are input to the simulation model and a set of model outputs is produced. In essence, these model evaluations create a mapping from the space of the inputs to the space

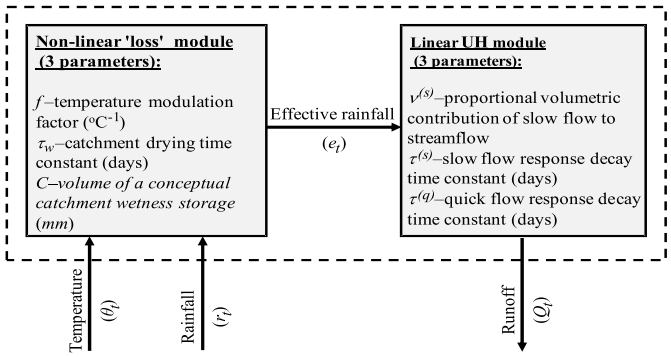

Fig. 2. Schematic of rainfall-runoff simulation in IHACRES.

of the results. This mapping is the basis for subsequent uncertainty and sensitivity analysis.

4. The results of model evaluations become the basis for uncertainty analysis. One approach to characterize the statistical uncertainty is with a mean value and a variance of results. Other model output statistics are provided.

SIMLAB is composed of three modules (Giglioli and Saltelli 2003): (1) the statistical preprocessor module, which executes the first and second steps; (2) the model execution module, which executes the third step; and (3) the statistical postprocessor module, which executes the fourth step.

Rainfall-Runoff Simulation

The IHACRES rainfall-runoff model was applied to simulate runoff in the Khorramabad River Basin under the impact of climate change. This model was introduced by Jakeman and Hornberger (1993). The IHACRES model is a lumped model in which input variables and parameters are uniform over the modeled area (Liu et al. 2006). IHACRES features nonlinear and linear modules (Fig. 2). IHACRES converts rainfall and temperature at each time step into effective rainfall using the nonlinear module, and the effective rainfall is converted into surface runoff in the same time step using the linear module. Three parameters τ_w, f, and c from the nonlinear module, and three parameters $v^{(s)}$, $\tau^{(s)}$, and $\tau^{(q)}$ from the linear module must be calibrated based on observed runoff data.

Results and Discussion

Geographical Location of Studied Area

The Khorramabad study area is located within Lorestan Province in western Iran. This study area is located between the eastern longitudes 55° 47′ through 50° 48′ and the northern latitudes 40° 32′ through 20° 34′. The Khorramabad study area consists of a main plain (central plain) and a number of small dispersed plains, such as Deh Par, Kamalvand, Khorramabad, and others which are connected to neighboring city centers through the Boroujerd–Khorramabad, Poldokhtar–Khorramabad, and Dorood–Khorramabad roads. The Khorramabad study area lies within the eastern part of the Karkheh Basin. It has an area of 2,501.4 km^2, of which 212.4 km^2 is plains and 2,289 km^2 is highlands. The area of the main plain is 133 km^2, and the areas of the Khorramabad, Kamalvand, and Deh Par plains are 22, 25.9, and 32.5 km^2, respectively. Fig. 3 displays the study area's location relative to Iran's watersheds.

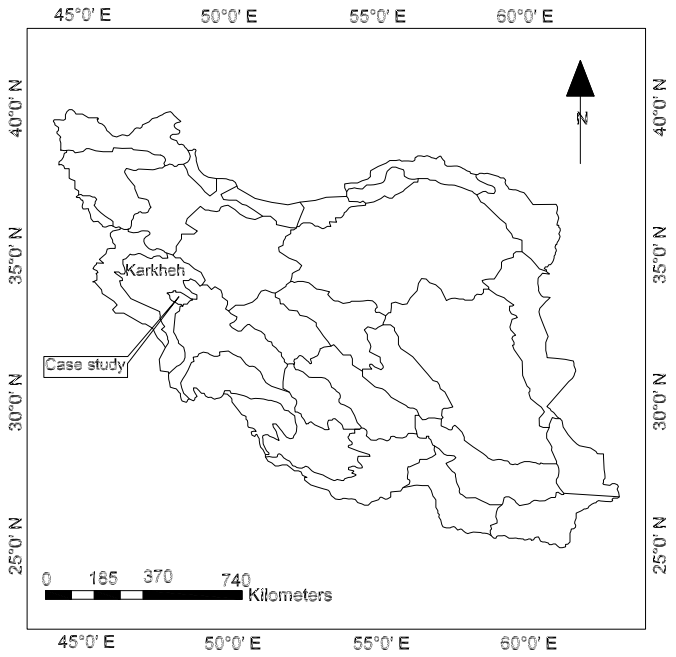

Fig. 3. Location of the study area relative to other Iranian watersheds.

The perennial Khorramabad River streamflow stems from rainfall excess, from spring flows, and from drainage issuing from the plains and highlands. The Duab-Visian hydrometric station is located near the outlet of the Khorramabad study area; measurements there began in 2001. It is not possible to estimate the streamflow using the relatively short recording period at this station. Therefore, this study estimated the runoff volume and total annual drainage from the region based on data collected at the Cham-anjir hydrometric station located in the middle section of the Khorramabad region. The stations' data include the period 1971–2000, and for this reason it was selected as the baseline period for analysis in this work.

Performance Assessment of the AOGCMs

The accuracy of the AOGCMs in simulating climatic variables in the baseline period 1971–2000 (when observed data are available) proved acceptable. Fig. 4 compares the 30-year average of the climate variables projected by the AOGCMs with the corresponding observed data.

Fig. 4 indicates that the HadCM3 simulations for the months of April–July overestimated the observed values for temperature under the A2 emission scenario, and in other months they underestimated the observed values. The CCSR-NIES model overestimated the observed values for almost all months except October–December. The CSIRO-MK2 model underestimated observed values for all months except April–June. The CGCM2 underestimated observed values for all months. The GFDL-R30 model overestimated the observed values for all months except November–March. Similar patterns of prediction held for the B2 emission scenario. All models underestimated observed values for rainfall under the A2 scenario in January, February, and March. Observed values were underestimated in all months by all models, except by the CGCM2 in April and May. The CGCM2 and CSIRO-MK2 models overestimated observed values in June, and the rest of the models underestimated the observed values in that month. Most models overestimated observed values in July–September. All models except HadCM3 underestimated the observed values in October–December. The results

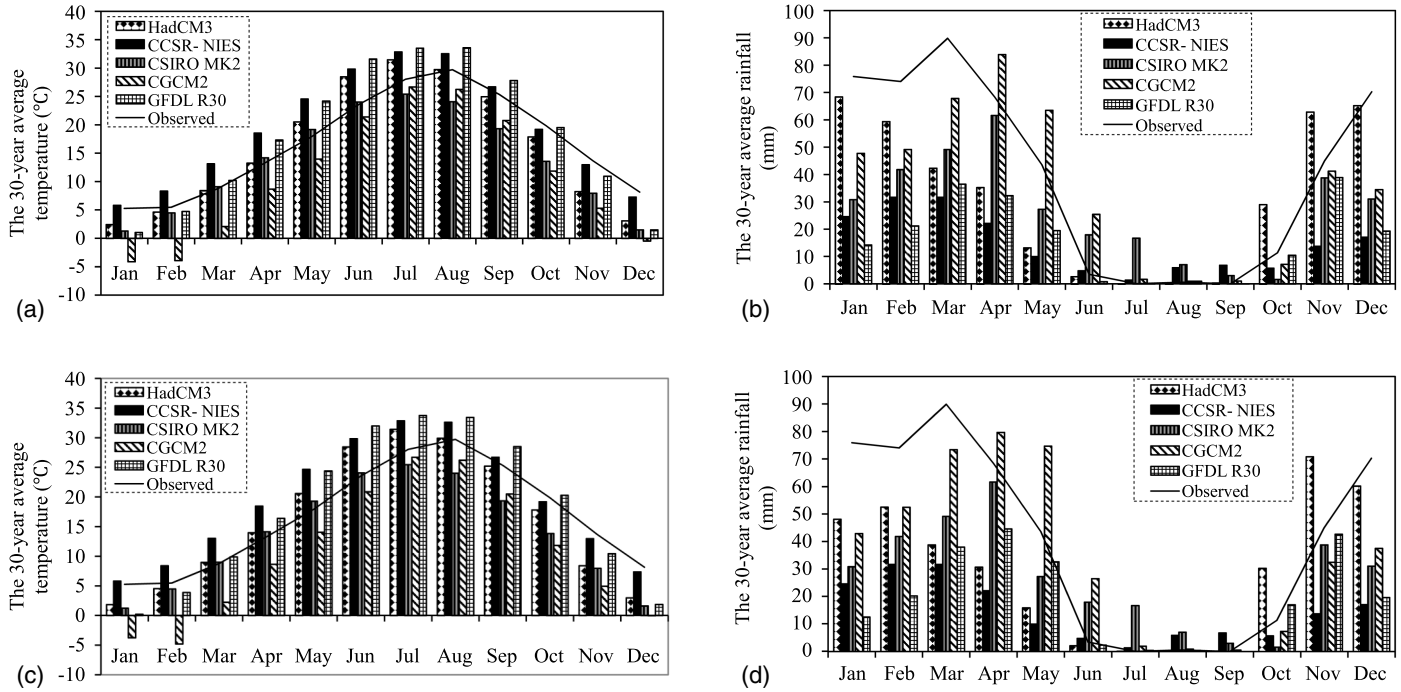

Fig. 4. Evaluation and comparison of the AOGCM outputs in the baseline period: (a) Scenario A2, temperature; (b) Scenario A2, rainfall; (c) Scenario B2, temperature; and (d) Scenario B2, rainfall.

for rainfall under B2 scenario had similar patterns of accuracy to those of scenario A2.

The performance accuracy was assessed with the coefficient of determination (R^2), root mean squared error (RMSE), mean absolute error (MAE), and Nash–Sutcliffe efficiency coefficient (NSE). The assessment results are listed in Table 1. The higher the coefficient of determination and the lower the error rate, the better is the performance of the model. The data in Table 1 for temperature under the A2 and B2 emission scenarios indicate that HadCM3 performed better than the other models. CGCM2 performed better than other models for rainfall under the A2 and B2 emission scenarios.

Calculation of Climate Change Scenarios in Future Periods

The accuracy of the AOGCMs in simulating climatic variables in the baseline period proved acceptable. Climate change scenarios for temperature and rainfall in the basin were calculated for the future period. The time series of temperature and rainfall projections from AOGCMs corresponding to the A2 and B2 emission scenarios were downscaled for the basin scale. The difference between average projected monthly temperature and average simulated monthly temperature in the baseline period and the ratio of average projected monthly rainfall to average simulated monthly rainfall in

Table 1. Assessment of accuracy of AOGCMs with performance criteria

Emission scenario	Climatic variable	Performance criteria	Models				
			HadCM3	CCSR-NIES	CSIRO MK2	CGCM2	GFDL R30
A2	Temperature	R^2 (%)	94.32	92.78	87.59	97.89	92.89
		RMSE (°C)	3.04	3.8	4.19	6.48	4.51
		MAE (°C)	2.33	3.1	3.4	5.87	3.86
		NSE	0.87	0.79	0.75	0.4	0.71
	Rainfall	R^2 (%)	68.44	87.13	71.02	70.25	63.19
		RMSE (mm)	20.81	35.34	24.55	19	34.1
		MAE (mm)	14.62	28.04	19.72	14.94	24.08
		NSE	0.62	0.1	0.47	0.68	0.03
B2	Temperature	R^2 (%)	94.21	92.84	87.79	97.7	93.73
		RMSE (°C)	3.08	3.81	4.15	6.56	4.64
		MAE (°C)	2.42	3.1	3.38	5.96	4.02
		NSE	0.87	0.79	0.76	0.39	0.69
	Rainfall	R^2 (%)	58.29	87.13	71.02	67.17	48.92
		RMSE (mm)	24.41	35.34	24.55	19.78	32.73
		MAE (mm)	18.55	28.04	19.72	15.71	21.97
		NSE	0.47	0.1	0.47	0.65	0.05

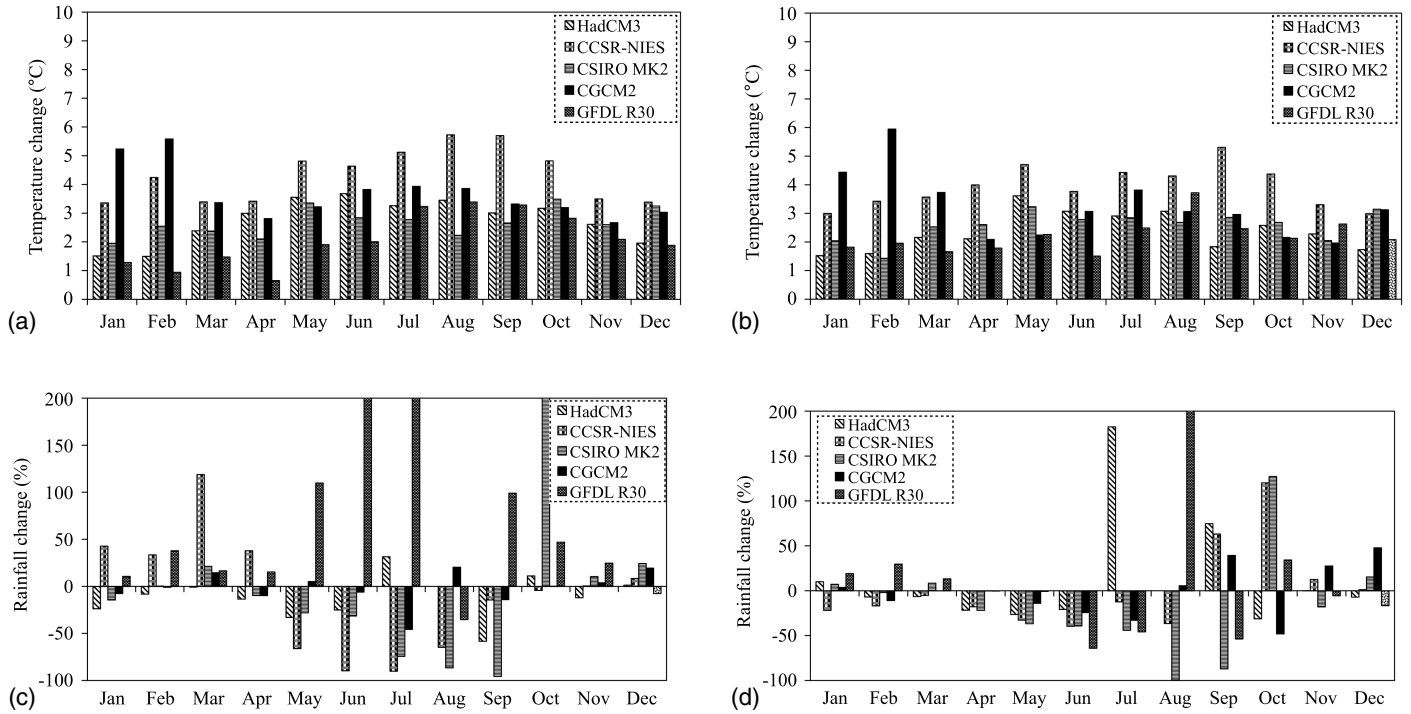

Fig. 5. Future projections (2040–2069) relative to baseline period: (a) Scenario A2, temperature; (b) Scenario B2, temperature; (c) Scenario A2, rainfall; and (d) Scenario B2, rainfall. The change projections are with respect to the average baseline values.

the baseline period were calculated. The results are portrayed in Figs. 5 and 6. All models projected temperatures for 2040–2069 higher than those in the baseline period (Fig. 5). The models projected an increase in temperature of between 0.65°C and 5.73°C and between 1.43°C and 5.95°C for the A2 and B2 emission scenarios, respectively. The HadCM3 and the CCSR-NIES temperature projections under the A2 scenario had smaller increases in the cold months and larger increases in the warm months. The CGCM2 temperature projections indicated that the temperature would increase during the cold and warm months by 5.58°C and 3.32°C,

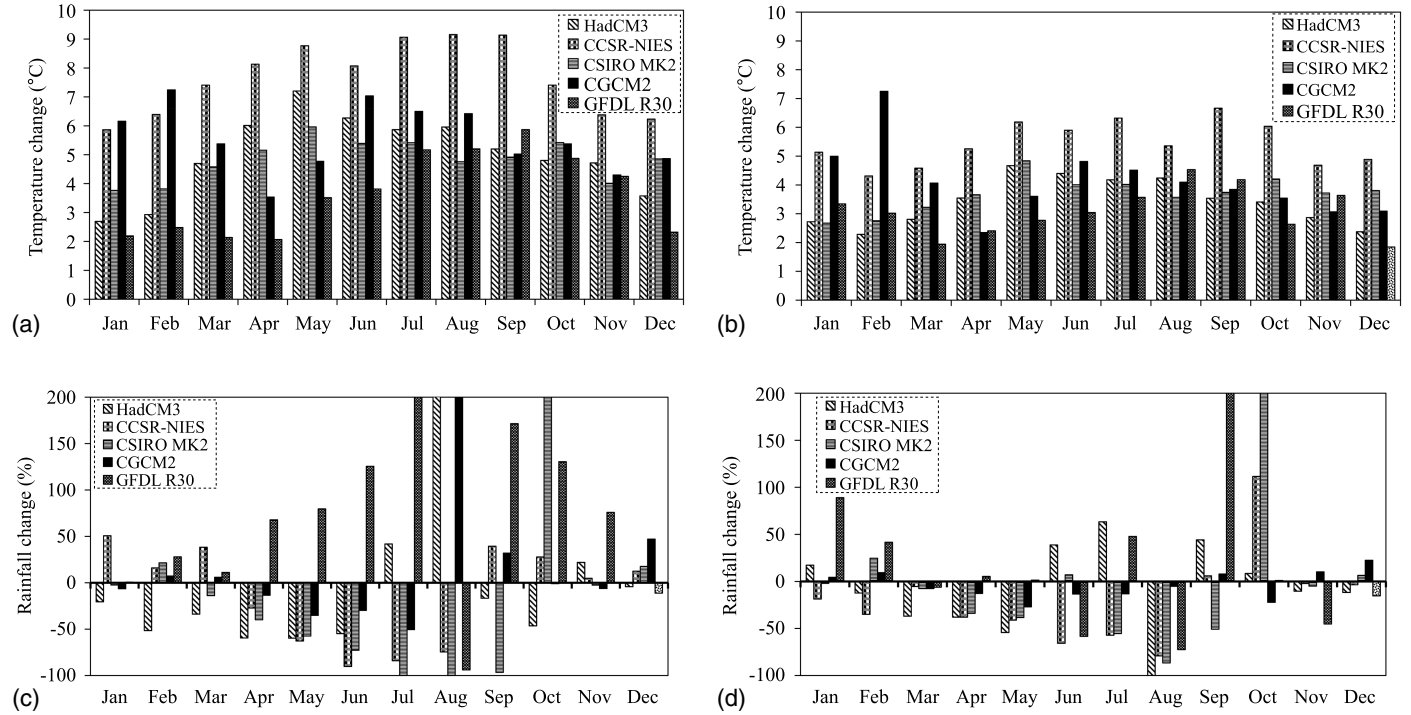

Fig. 6. Future projection (2070–2099) relative to baseline period: (a) Scenario A2, temperature; (b) Scenario B2, temperature; (c) Scenario A2, rainfall; and (d) Scenario B2, rainfall. The change projections are with respect to the average baseline values.

respectively. GFDLR30 projected an increase in temperature for almost all months, although the increase was smaller than in the baseline period, except for the summer season. CSIRO MK2 projected lower temperatures in the future than in the baseline period. The HadCM3 and the CCSR-NIES models, in that decreasing order, provided the best temperature projections corresponding to the A2 and B2 emissions scenarios. CGCM2 projected an increase in temperature of 5.95°C and 2.96°C in the cold and warm months, respectively. Comparing emission scenarios, the B2 scenario had a larger increase in temperature. The largest temperature rise corresponded to CGCM2 in February, 5.95°C, and the smallest temperature rise corresponded to GFDL-R30 in April, 0.65°C. Concerning rainfall projections associated with the A2 and B2 scenarios, some models indicated increases and some indicated decreases for some months. The rainfall change ranged between −95.63% and 209.35% for Scenario A2 [Fig. 5(c)], and between −99.39% and 219.81% for Scenario B2 [Fig. 5(d)]. GFDL-R30 produced the smallest range of change for both emissions scenarios, and CGCM2 exhibited the largest range of change among the models. Most models projected increasing rainfall in the autumn and decreasing rainfall in the summer for Emissions Scenarios A2 and B2.

In the periods 2070-2099 and 2040-2069, all models projected temperatures higher than in the baseline period, so that under the A2 scenario [Fig. 6(a)] temperature increased by between 2.07°C and 9.15°C, and under the B2 scenario [Fig. 6(b)] it increased by between 1.85°C and 7.25°C. The CCSR-NIES model predicted higher temperature than did the other models in most months under Scenarios A2 and B2. The projected temperature increase was higher in the warm months under both emission scenarios according to most AOGCMs. Most models projected lower rainfall in spring and summer under Scenarios A2 and B2, and they projected more rainfall in autumn and winter under both scenarios. Comparison of the projected temperatures indicates that both emission scenarios projected higher temperature in the period 2070–2099 than in the period 2040–2069. In addition, comparing rainfall for both scenarios shows that the models had a lower range of prediction values in the period 2070–2099 than in 2040–2069.

Monte Carlo Simulation Results

The monthly $\Delta\theta$ (change in temperature) and Δr (change in rainfall) extracted from the AOGCMs were weighted for every month (average long-term) (Fig. 7). The higher the weight of the model, the greater is the effect of that model on the projections of temperature and rainfall. For temperature under the A2 scenario, the largest weight corresponded to HadCM3, and the smallest corresponded

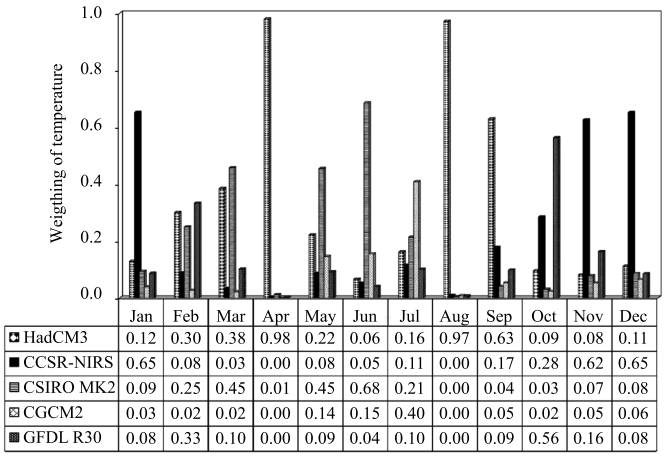

	Jan	Feb	Mar	Apr	May	Jun	Jul	Aug	Sep	Oct	Nov	Dec
HadCM3	0.12	0.30	0.38	0.98	0.22	0.06	0.16	0.97	0.63	0.09	0.08	0.11
CCSR-NIRS	0.65	0.08	0.03	0.00	0.08	0.05	0.11	0.00	0.17	0.28	0.62	0.65
CSIRO MK2	0.09	0.25	0.45	0.01	0.45	0.68	0.21	0.00	0.04	0.03	0.07	0.08
CGCM2	0.03	0.02	0.02	0.00	0.14	0.15	0.40	0.00	0.05	0.02	0.05	0.06
GFDL R30	0.08	0.33	0.10	0.00	0.09	0.04	0.10	0.00	0.09	0.56	0.16	0.08

(a)

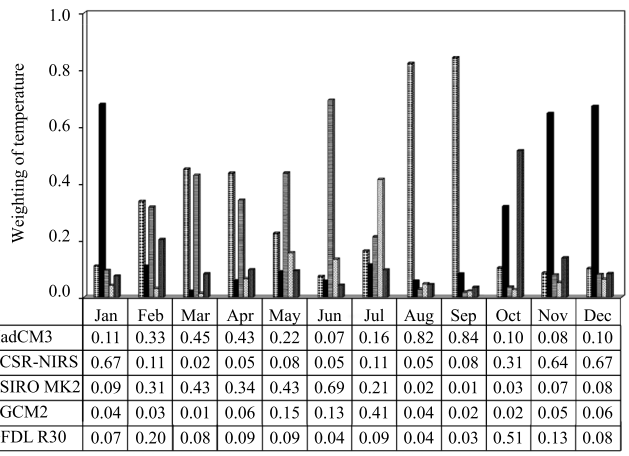

	Jan	Feb	Mar	Apr	May	Jun	Jul	Aug	Sep	Oct	Nov	Dec
HadCM3	0.11	0.33	0.45	0.43	0.22	0.07	0.16	0.82	0.84	0.10	0.08	0.10
CCSR-NIRS	0.67	0.11	0.02	0.05	0.08	0.05	0.11	0.05	0.08	0.31	0.64	0.67
CSIRO MK2	0.09	0.31	0.43	0.34	0.43	0.69	0.21	0.02	0.01	0.03	0.07	0.08
CGCM2	0.04	0.03	0.01	0.06	0.15	0.13	0.41	0.04	0.02	0.02	0.05	0.06
GFDL R30	0.07	0.20	0.08	0.09	0.09	0.04	0.09	0.04	0.03	0.51	0.13	0.08

(b)

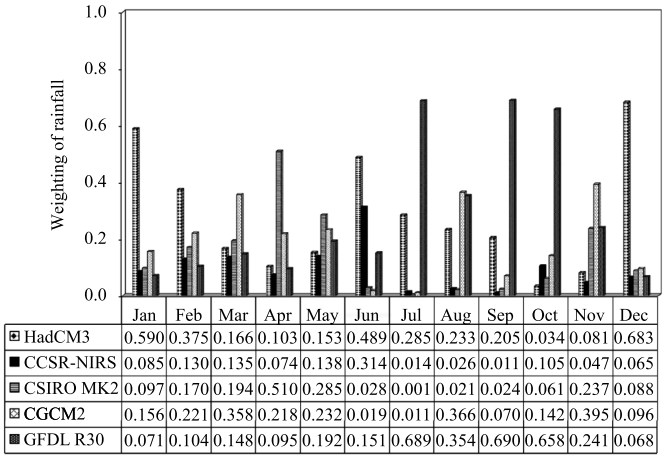

	Jan	Feb	Mar	Apr	May	Jun	Jul	Aug	Sep	Oct	Nov	Dec
HadCM3	0.590	0.375	0.166	0.103	0.153	0.489	0.285	0.233	0.205	0.034	0.081	0.683
CCSR-NIRS	0.085	0.130	0.135	0.074	0.138	0.314	0.014	0.026	0.011	0.105	0.047	0.065
CSIRO MK2	0.097	0.170	0.194	0.510	0.285	0.028	0.001	0.021	0.024	0.061	0.237	0.088
CGCM2	0.156	0.221	0.358	0.218	0.232	0.019	0.011	0.366	0.070	0.142	0.395	0.096
GFDL R30	0.071	0.104	0.148	0.095	0.192	0.151	0.689	0.354	0.690	0.658	0.241	0.068

(c)

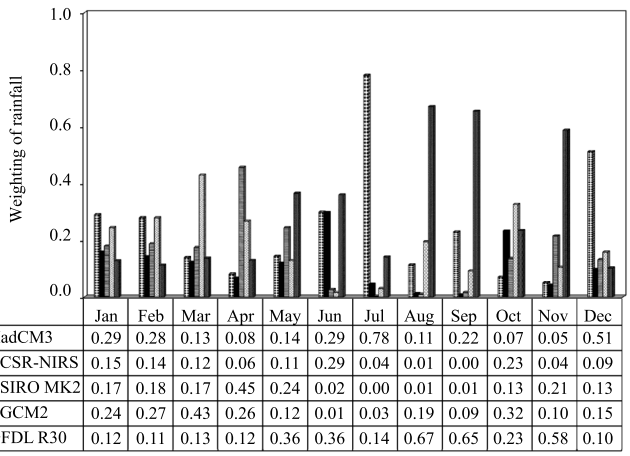

	Jan	Feb	Mar	Apr	May	Jun	Jul	Aug	Sep	Oct	Nov	Dec
HadCM3	0.29	0.28	0.13	0.08	0.14	0.29	0.78	0.11	0.22	0.07	0.05	0.51
CCSR-NIRS	0.15	0.14	0.12	0.06	0.11	0.29	0.04	0.01	0.00	0.23	0.04	0.09
CSIRO MK2	0.17	0.18	0.17	0.45	0.24	0.02	0.00	0.01	0.01	0.13	0.21	0.13
CGCM2	0.24	0.27	0.43	0.26	0.12	0.01	0.03	0.19	0.09	0.32	0.10	0.15
GFDL R30	0.12	0.11	0.13	0.12	0.36	0.36	0.14	0.67	0.65	0.23	0.58	0.10

(d)

Fig. 7. Modes weighting for the climate change projections: (a) Scenario A2, temperature; (b) Scenario B2, temperature; (c) Scenario A2, rainfall; and (d) Scenario B2, rainfall.

to the CCSR-NIES and CGCM2 models. The largest weight for Scenario B2 corresponded to HadCM3, and the smallest weight corresponded to CSIRO-MK2. Rainfall projections under the A2 scenario indicated that the largest weights corresponded to the HadCM3 and GFDL-R30 models, and the smallest weight corresponded to CSIRO-MK2. Rainfall projections under the B2 scenario showed that the largest weight was associated with HadCM3 and the smallest weight corresponded to CSIRO-MK2. In general, HadCM3 had the greatest effect on temperature and rainfall for emission scenarios A2 and B2, and, therefore, it had the largest impact on future runoff.

Table 2. Performance criteria for IHACRES model

Time period	R^2 (%)	RMSE (m^3/s)	MAE (m^3/s)	NSE
1971–1990 (calibration)	68.4	4.98	3.37	0.66
1991–2000 (verification)	67.4	5.78	4.27	0.64
1971–2000 (total period)	67.3	5.26	3.67	0.65

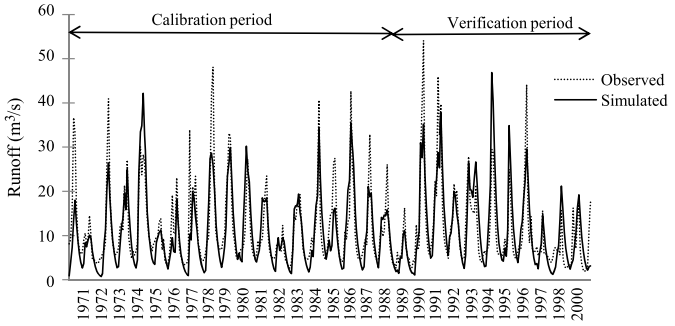

Fig. 8. Comparison of simulated and observed runoff in the period 1971–2000.

The models were weighed with respect to $\Delta\theta$ and Δr. Following that, the monthly probability distribution functions of $\Delta\theta$ and Δr were calculated. Lastly, 100 samples of $\Delta\theta$ and Δr were generated from each monthly probability distribution function by means of Monte Carlo simulation and SIMLAB software. Subsequently, 100 time series of monthly temperature and rainfall were generated.

Calibration and Validation Results for Rainfall-Runoff Model

The IHACRES model was calibrated and validated with the average monthly rainfall and temperature data and the monthly runoff recorded at Cham-anjir station during the period 1971–2000. Table 2 lists the calibration and validation results, which show that the calibration period 1971–1990 had excellent accuracy performance. The period 1991–2000 served for validating the IHACRES model. Fig. 8 displays the riverflow time series for the entire period 1971–2000. Results showed the model has acceptable performance in runoff prediction. The results listed in Table 2 indicate that the R^2 in the calibration and validation periods was high and the error rates were low. This provides ample evidence that the IHACRES model has good predictive skill for river flow simulation. Fig. 8 shows that

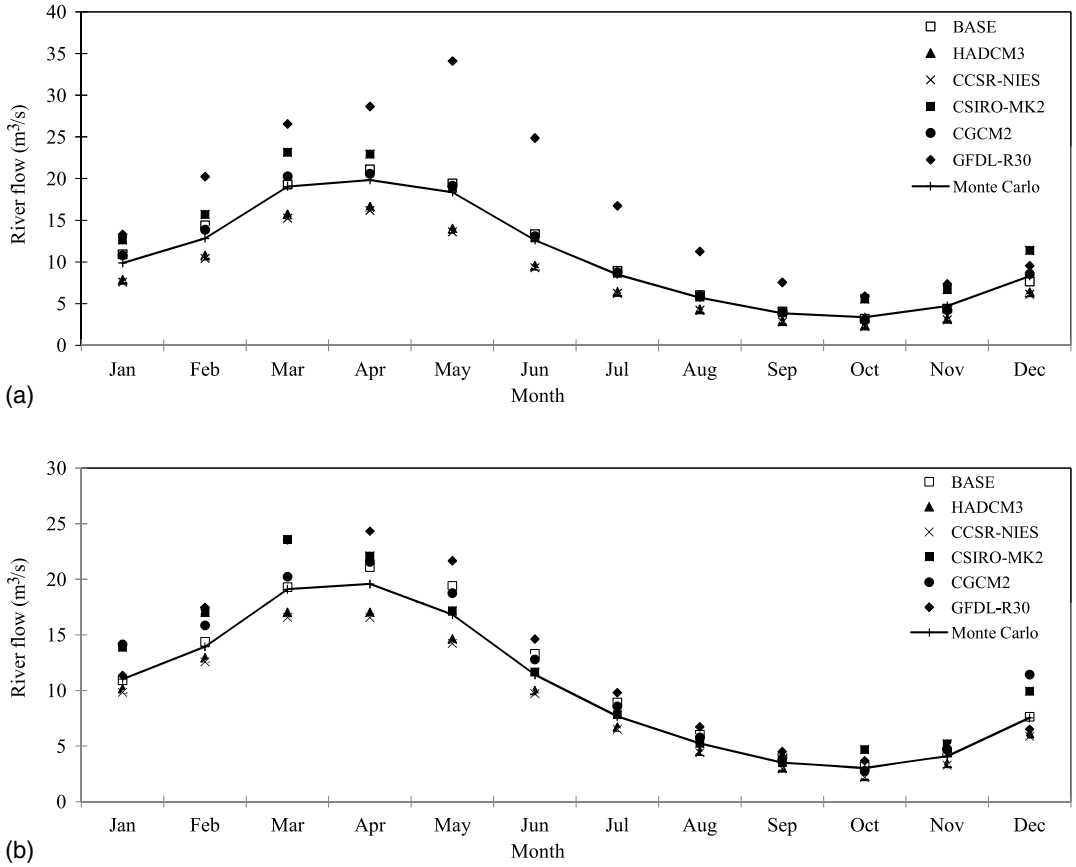

Fig. 9. Comparison of monthly long-term river flow (runoff) from several AOGCMs and Monte Carlo simulation in the period 2040–2069 with baseline values for (a) Scenario A2; and (b) Scenario B2.

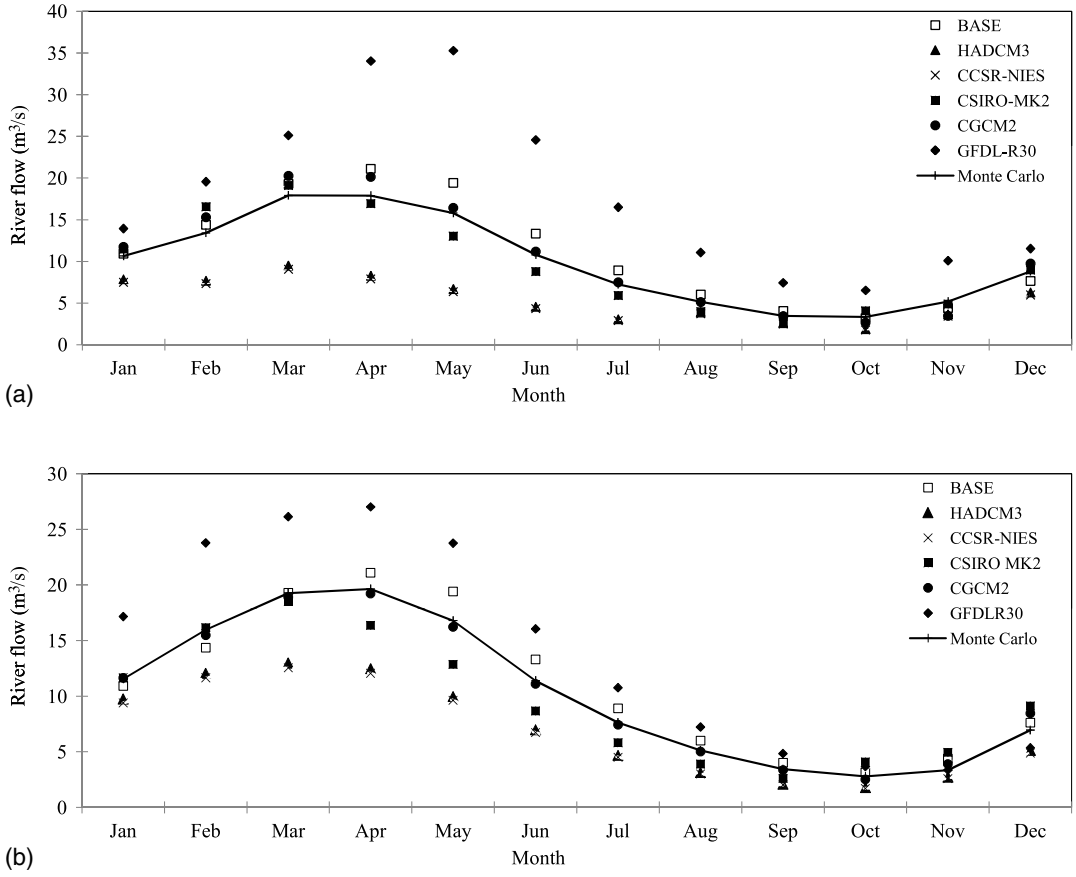

Fig. 10. Comparison of monthly long-term river flow (runoff) from several AOGCMs and Monte Carlo simulation in the period 2070–2099 with baseline values for (a) Scenario A2; and (b) Scenario B2.

in the calibration period 1971–1990 and the verification period 1991–2000, the simulated runoff was close to the observed runoff.

Simulation of River Flow in Future Periods

Monthly time series of river flow were simulated with the IHACRES model and the climatic data from (1) five AOGCMs; and (2) the average of the 100 monthly time series generated by Monte Carlo simulation. The average monthly river flow of these six time series projected over the future periods were compared with the baseline variables under Scenarios A2 and B2. The results are presented in Figs. 9 and 10.

Under emission scenarios A2 and B2 and in periods 2069–2040 and 2070–2099, the developed Monte Carlo model's river-flow projections fit well the projections by the AOGCMs. The AOGCMs' river-flow projections under the B2 scenario were closer to each other than those under the A2 scenario. A comparison of future projections established that the AOGCMs' predictions for the period 2040–2069 were closer to each other than those for 2070–2099. The river-flow projections established that GFDLR30 exhibited the least accurate results among the AOGCMs. Furthermore, comparison of Figs. 9 and 10 shows that the AOGCMs' river-flow projections were closer to each other in the summer and autumn.

Concluding Remarks

This work assessed the effects of climate change on the runoff of the Khorramabad River Basin in Lorestan Province, Iran. Five AOGCM climatic projections (HadCM3, CCSR-NIES, CSIRO-MK2, CGCM2, and GFDL-R30) for the periods 2040–2069 and 2070–2099 and under IPCC Scenarios A2 and B2 were employed in this work's assessment of future runoff in the study area.

The HadCM3 and CGCM2 projections were found to be most accurate compared with the baseline temperature and rainfall, respectively, judged by R^2, RMSE, MAE, and NSE criteria. The AOGCMs' projections indicated an increase in temperature and a decrease in rainfall in the future periods, such that the temperature of the basin in the period 2040–2069 under the A2 and B2 scenarios increased by between 0.65°C and 5.73°C and between 1.43°C and 5.95°C, respectively, and in the period 2070–2099 under the A2 and B2 scenarios it increased by between 2.07°C and 9.15°C and between 1.85°C and 7.25°C, respectively, relative to the baseline period. Furthermore, the range of rainfall change in the period 2040–2069 under the A2 and B2 scenarios was between −95.63% and 209.35% and between −99.39% and 219.81%, respectively, and in the period 2070-2099 under the A2 and B2 scenarios it was respectively between −99.85% and 206% and between −100% and 203.20%. One hundred time series of downscaled temperature and rainfall were generated with the Monte Carlo method based on their probability distribution functions. The IHACRES model was calibrated and validated, and climatic data from (1) five AOGCMs, and (2) the developed Monte Carlo model were input to the IHACRES model to simulate future river flow. Our results indicate the average annual runoff in the period 2040–2069 under the A2 and B2 scenarios decreased by 7.76% and 10.63%, respectively, and decreased in the period 2070–2099 under the A2 and B2 scenarios by 13.06% and 29.49%, respectively. These results indicate a

worsening availability of runoff through the remainder of the 21st century in the study region.

The uncertainties of the different hydrological models, downscaling methods, and emission scenarios influence runoff projections. This work included a downscaling method (i.e., method of interpolation due to its simple implementation), a hydrological model (i.e., IHACRES), and a weighting technique (because of its simplicity and accuracy) for the purpose of projecting climate change impacts on river flow using four performance criteria. The projections yield a first scenario for adapting future water resources management in the study region. More complex assessment of uncertainties will be the subject of future research.

Table 3. Specifications of meteorological stations located in study area

Number	Station code	Station name	River basin	Geographic characteristics			Year of establishment	Type of station
				Longitude	latitude	Elevation (m)		
1	221011002	Tang Valley	Ab-shotor	48–16	33–56	1,730	1373	Evaporation gauge
2	220613006	Paul Keshkan	Khashkan	47–48	33–30	960	1346	Rain gauge
3	221113001	Kakarza	Harud	48–16	33–43	1,550	1345	Rain gauge
4	221013001	Seyed Ali	Ab-shotor	48–13	33–48	1,530	1345	Rain gauge
5	233813003	Sarkhab	Sezar	48–38	33–08	770	1343	Rain gauge
6	221313001	Tang-Siab	Ab-Siah	47–12	32–23	940	1349	Rain gauge
7	220811002	Cham-anjir	Khorramabad	48–14	33–27	1,166	1368	Evaporation gauge
8	233911011	Rahim-abad	Chalan Chulan	48–48	33–14	1,490	1365	Evaporation gauge
9	221211005	Gol-Zard	Seimareh	47–21	33–11	680	1368	Evaporation gauge
10	222011001	Hulilan	Humian	47–15	33–44	1,000	1350	Evaporation gauge
11	2206121001	Poledokhtar	Payab Kashkan	47–43	33–10	700	1345	Rain gauge
12	233813009	Cham-chit	Goharrud	48–59	33–23	1,290	1343	Evaporation gauge
13	233811006	Sepid-dasht	Sezar	48–53	33–47	970	1356	Evaporation gauge
14	220713001	Kuh-dasht	Madian-rud	47–37	33–32	970	1373	Rain gauge
15	233913005	Durud	Tireh	49–04	33–29	1,450	1343	Evaporation gauge
16	221313001	Dehnu	Harude	48–46	33–30	1,800	1383	Rain gauge
17	220613004	Afarineh	Cholhul	47–54	33–20	820	1345	Rain gauge
18	220613003	Afarineh	Kashkan	47–54	33–20	820	1345	Rain gauge
19	—	Khoramabad	Khoramabad	48–17	33–26	1,147.8	1377	Synoptic

Table 4. Annual statistical indexes of river flow

Model	Period	Emission scenario	Annual river flow		
			Average (m^3/s)	Standard deviation (m^3/s)	Coefficient of variation (%)
HadCM3	1971–2000	—	11.05	6.14	1.8
	2040–2069	A2	8.33	4.81	1.73
		B2	8.99	5.19	1.73
	2070–2099	A2	5.47	2.42	2.26
		B2	6.98	4.09	1.71
CCSR-NIES	1971–2000	—	11.05	6.14	1.8
	2040–2069	A2	8.08	4.68	1.73
		B2	8.72	5.06	1.72
	2070–2099	A2	5.21	31.2	2.25
		B2	6.73	3.96	1.7
CSIRO-MK2	1971–2000	—	11.05	6.14	1.8
	2040–2069	A2	12.34	6.4	1.93
		B2	11.81	6.64	1.78
	2070–2099	A2	9.68	5.44	1.78
		B2	9.56	5.26	1.82
CGCM2	1971–2000	—	11.05	6.14	1.8
	2040–2069	A2	11.01	6.14	1.79
		B2	11.7	6.32	1.85
	2070–2099	A2	10.57	6.1	1.73
		B2	10.28	5.83	1.76
GFDL-R30	1971–2000	—	11.05	6.14	1.8
	2040–2069	A2	17.16	9.13	1.88
		B2	12.39	7.4	1.68
	2070–2099	A2	17.96	9.43	1.9
		B2	10.14	8.93	1.58
Developed Monte	1971–2000	—	11.05	6.14	1.8
Carlo model	2040–2069	A2	10.57	5.71	1.85
			10.24	5.76	1.78
	2070–2099	B2	9.96	5.12	1.95
			10.33	6.06	1.7

Table 5. Projected runoff minus baseline runoff for different AOGCMs and Monte Carlo method (%)

Model	Percentage change in runoff			
	A2-2040-2069	A2-2070-2099	B2-2040-2069	B2-2070-2099
HadCM3	−27.29	−52.23	−21.55	−39.06
CCSR-NIES	−29.49	−54.49	−23.89	−41.25
CSIRO-MK2	+7.74	−15.5	+3.06	−16.52
CGCM2	+3.88	−7.76	+2.15	−10.31
GDFL-R30	+49.78	+56.72	+8.1	+23.05
Developed Monte Carlo model	−7.76	−13.06	−10.63	−29.49

Appendix. Supplemental Information

The characteristics of the hydrometric stations located in the study area are listed in Table 3.

The uncertainty of AOGCMs' river-flow projections was assessed with statistical indicators (Table 4). The CCSR-NIES projected river flow decreased by 36.76% and 26.72% in 2040–2069 under the A2 and B2 scenarios, respectively, and it decreased by 112.09% and 64.19% in 2070–2099 under the A2 and B2 scenarios, respectively. The CGCM2 projected runoff (river flow) decreased by 0.36% in 2040–2069 under the A2 scenario, and it increased by 5.56% under the B2 scenario. Runoff decreased by 4.54% and 7.49% in 2070–2099 under the A2 and B2 scenarios, respectively. The CSIRO-MK2 projected runoff increased by 10.45% and 6.44% in 2040–2069 under the A2 and B2 scenarios, respectively, and it decreased by 14.15% and 15.59% in 2070–2099 under the A2 and B2 scenario, respectively. The GFDL-R30 model projected runoff increased by 35.61% and 10.82% in 2040–2069 under the A2 and B2 scenarios, respectively, and it increased by 38.47% in 2070–2099 under the A2 scenario and decreased by 8.97% under the B2 scenario. The HadCM3 projected runoff decreased by 32.65% and 22.91% in 2040–2069 under the A2 and B2 scenarios, respectively, and it decreased by 102.01% and 58.31% for 2070–2099 under the A2 and B2 scenario, respectively. The model developed by Monte Carlo simulations projected that the runoff will decrease by 4.54% and 7.91% in 2040-–2069 under the A2 and B2 scenarios, respectively, and it will decrease by 10.94% and 6.97% in 2070–2099 under the A2 and B2 scenarios, respectively.

The runoff (river flow) changes with respect to baseline values projected by the AOGCMs and the developed model by the Monte Carlo method under the A2 and B2 scenarios in the periods 2040–2069 and 2070–2099 are listed in Table 5. The preponderance of the projections indicated reduced future runoff in the study region, except for the GFDL30 projections.

References

Ahmadi, M., O. Bozorg-Haddad, and M. A. Mariño. 2014. "Adaptive reservoir operation rules under climatic change." *Water Resour. Manage.* 29 (4): 1147–1266. https://doi.org/10.1007/s11269-014-0871-0.

Ashofteh, P.-S., O. Bozorg-Haddad, and H. A. Loáiciga. 2016a. "Development of adaptive strategies for irrigation water demand management under climate change." *J. Irrig. Drain. Eng.* 143 (2): 04016077. https://doi.org/10.1061/(ASCE)IR.1943-4774.0001123.

Ashofteh, P.-S., O. Bozorg-Haddad, and M. A. Mariño. 2013. "The impact of climate change on reservoir performance indices in agricultural water supply." *J. Irrig. Drain. Eng.* 139 (2): 85–97. https://doi.org/10.1061/(ASCE)IR.1943-4774.0000496.

Ashofteh, P.-S., O. Bozorg-Haddad, and M. A. Mariño. 2016b. "Performance evaluation of a developed hybrid AOGCM model under climate change." *J. Irrig. Drain. Eng.* 142 (12): 04016068. https://doi.org/10.1061/(ASCE)IR.1943-4774.0001107.

Barrow, E., M. Hulme, and M. Semenov. 1996. "Effect of using different methods in the construction of climate change scenarios: Examples from Europe." *Clim. Res.* 7 (3): 195–211. https://doi.org/10.3354/cr007195.

Chau, K. W. 2007. "A split-step particle swarm optimization algorithm in river stage forecasting." *J. Hydrol.* 346 (3–4): 131–135. https://doi.org/10.1016/j.jhydrol.2007.09.004.

Cheng, C. T., X.-Y. Wu, and K.-W. Chau. 2005. "Multiple criteria rainfall-runoff model calibration using a parallel genetic algorithm in a cluster of computer." *Hydrol. Sci. J.* 50 (6): 1069–1087. https://doi.org/10.1623/hysj.2005.50.6.1069.

Chithra, N. R., and S. G. Thampi. 2015. "Detection and attribution of climate change signals in precipitation in the Chaliyar River Basin, Kerala, India." *Aquat. Procedia* 4: 755–763. https://doi.org/10.1016/j.aqpro.2015.02.158.

Ekström, M., H. J. Fowler, C. G. Kilsby, and P. D. Jones. 2005. "New estimates of future changes in extreme rainfall across the UK using regional climate model integrations. 2. Future estimates and use in impact studies." *J. Hydrol.* 300 (1–4): 234–251. https://doi.org/10.1016/j.jhydrol.2004.06.019.

Fotovatikhah, F. H., M. Herrera, S. Shamshirband, K.-W. Chau, S. Fsizollahzadeh Ardabili, and M. Jalil Piran. 2018. "Survey of computational intelligence as basis to big flood management: Challenges, research directions and future work." *Eng. Appl. Comput. Fluid Mech.* 12 (1): 411–437. https://doi.org/10.1080/19942060.2018.1448896.

Gholami, V., K.-W. Chau, F. Fadaee, J. Torkaman, and A. Ghaffari. 2015. "Modeling of groundwater level fluctuations using dendrochronology in alluvial aquifers." *J. Hydrol.* 529 (3): 1060–1069. https://doi.org/10.1016/j.jhydrol.2015.09.028.

Giglioli, N., and A. Saltelli. 2003. *SIMLAB 2.2: Software for sensitivity and uncertainty analysis: SIMLAB manual*. Brussels, Belgium: Joint Research Centre, European Commission.

IPCC (Intergovernmental Panel on Climate Change). 2000. *Special report on emission scenarios*, 18. Geneva: IPCC.

IPCC (Intergovernmental Panel on Climate Change). 2001. "Summary for policymakers." In *Climate change 2001: Impacts, adaptation, and vulnerability, contribution of working group II to the third assessment report of the Intergovernmental Panel on Climate Change*, edited by J. J. McCarthy, O. F. CanzianiN. A. Leary, D. J. Dokken, and K. S. White, 1–17. Cambridge, UK: Cambridge University Press.

IPCC (Intergovernmental Panel on Climate Change). 2007. "Summary for policymakers." In *Climate Chang 2007: The physical science basis: Contribution of working group I to the fourth assessment report of the Intergovernmental Panel on Climate Change*, 18. Cambridge, UK: Cambridge University Press.

IPCC-TGCIA (Intergovernmental Panel on Climate Change-Task Group on Scenarios for Climate Impact Assessment). 1999. *Guidelines on the use of scenario data for climate impact and adaptation assessment: Version 1*, edited by T. R. Carter, M. Hulme, and M. Lal, 69. Geneva: IPCC-TGCIA.

Jakeman, A. J., and G. M. Hornberger. 1993. "How much complexity is warranted in a rainfall-runoff model?" *Water Resour. Res.* 29 (8): 2637–2649. https://doi.org/10.1029/93WR00877.

Jones, P. D., and M. Hulme. 1996. "Calculating regional climatic time series for temperature and precipitation: Methods and illustrations." *Int. J. Climatol.* 16 (4): 361–377. https://doi.org/10.1002/(SICI)1097-0088(199604)16:4<361::AID-JOC53>3.0.CO;2-F.

Lane, M. E., P. H. Kirshen, and R. M. Vogel. 1999. "Indicators of impact of global climate change on U.S. water resources." *J. Water Resour. Plann. Manage.* 125 (4): 194–204. https://doi.org/10.1061/(ASCE)0733-9496(1999)125:4(194).

Liu, Y. B., J. Corluy, A. Bahremand, F. D. Smedt, J. Poorova, and L. Velcická. 2006. "Simulation of runoff and phosphorus transport in a Carpathian catchment, Slovakia." *River Res. Appl.* 22 (9): 1009–1022. https://doi.org/10.1002/rra.953.

Mimikou, M., E. Baltas, and E. Varanou. 2001. "Climate change impacts on water resources: Quantity and quality aspects". In *Proc., World Environmental and Water Resources Congress*. Reston, VA: ASCE.

Mitchell, T. D. 2003. "Pattern scaling: An examination of the accuracy of the technique for describing future climates." *Clim. Change* 60 (3): 217–242. https://doi.org/10.1023/A:1026035305597.

Nakicenovic, N., and R. Swart. 2000. *Emissions scenarios: Special report of the Intergovernmental Panel on Climate Change*. Cambridge, UK: Cambridge University Press.

Nazif, S., M. Karamouz, and Z. Zahmatkesh. 2012. "Climate change impacts on runoff evaluation: A case study." In *Proc., World Environmental and Water Resources Congress*. Reston, VA: ASCE.

Prudhomme, C., D. Jakob, and C. Svensson. 2003. "Uncertainty and climate change impact on the flood regime of small UK catchments." *J. Hydrol.* 277 (1–2): 1–23. https://doi.org/10.1016/S0022-1694(03)00065-9.

Sarzaeim, P., O. Bozorg-Haddad, A. Bozorgi, and H. A. Loáiciga. 2017. "Runoff projection under climate change conditions with data-mining methods." *J. Irrig. Drain. Eng.* 143 (8): 04017026. https://doi.org/10.1061/(ASCE)IR.1943-4774.0001205.

Shah Karami, N., S. Morid, A. R. Massah Bavani, and M. Agha Alikhani. 2011. "Risk analysis and integrated water resources management based adaptation strategies for Zayandeh Rud irrigation system, Iran." In *Proc., 21st Int. Congress on Irrigation and Drainage (ICID)*. New Delhi, India: International Commission on Irrigation and Drainage.

Sidhu, R. S., K. Vatta, and U. Lall. 2011. "Climate change impact and management strategies for sustainable water-energy-agriculture outcomes in Punjab." *Indian J. Agric. Econ.* 66 (3): 328–339.

Taormina, R., K.-W. Chau, and B. Sivakumar. 2015. "Neural network river forecasting through baseflow separation and binary-coded swarm optimization." *J. Hydrol.* 529 (3): 1788–1797. https://doi.org/10.1016/j.jhydrol.2015.08.008.

von Storch, H., E. Zorita, and U. Cubasch. 1993. "Downscaling of global climate change estimation to regional scales: An application to Iberian rainfall in wintertime." *J. Clim.* 6: 1161–1171. https://doi.org/10.1175/1520-0442(1993)006<1161:DOGCCE>2.0.CO;2.

Wilby, R. L., and I. Harris. 2006. "A framework for assessing uncertainties in climate change impacts: Low flow scenarios for the River Thames, UK." *Water Resour. Res.* 42 (2): 1–10. https://doi.org/10.1029/2005WR004065.

Wu, C. L., and K.-W. Chau. 2011. "Rainfall-runoff modeling using artificial neural network coupled with singular spectrum analysis." *J. Hydrol.* 399 (3–4): 394–409. https://doi.org/10.1016/j.jhydrol.2011.01.017.

Zamani, R., A. M. Akhond-Ali, I. Ahmadianfar, and N. Ahmed Elagib. 2017. "Optimal reservoir operation under climate change based on a probabilistic approach." *J. Hydrol. Eng.* 22 (10): 05017019. https://doi.org/10.1061/(ASCE)HE.1943-5584.0001559.